Acta Cryst. (1980). A**36**, 89–96

An X-ray Investigation of the High-Temperature Phase of K_2SnCl_6

BY J. IHRINGER

Institut für Kristallographie der Universität Tübingen, Charlottenstrasse 33, *D*-7400 *Tübingen, Federal Republic of Germany*

(*Received* 4 *April* 1979; *accepted* 6 *August* 1979)

Abstract

At room temperature the background of X-ray single-crystal photographs exhibits diffuse streaks along the line Δ from Γ to X and less sharp diffuse domains in the directions Σ. The streaks are explained by a soft rotary phonon $A_2(\Delta)$ corresponding to an in-phase rotation of the octahedra in a plane. The displacements of the Cl ions due to their librations are identified in a difference-Fourier chart. The second diffuse system is explained by a transversal accoustical mode $B_1(\Sigma)$. The in-phase rotation of the octahedra in a plane minimizes the electrostatic energy, independently of the phase of the rotation in adjacent planes. In the model the repulsive parameter between the Cl and K ions decides whether the space group $P4/mnc$, as a result of an $A_{2g}(X)$ condensation, or the orthorhombic $Pnnn$, as a result of a second rotary mode condensation, is energetically favorable.

1. Introduction

Crystals of the chemical compositon R_2MX_6 having the cubic antifluorite structure (Fig. 1) may be thought of as being composed of 'isolated' MX_6 octahedra which are centered in the (000) position of a f.c.c. lattice. The R ions at $(\frac{1}{4},\frac{1}{4},\frac{1}{4})$ are surrounded by MX_6 octahedra in a tetrahedral coordination. For K_2SnCl_6, the compound we are concerned with here, all the structural information necessary is contained in Table 1. Two parameters are sufficient to describe the geometrical aspects of the structure: the lattice constant a_0 and the position of the chlorine ion, (u00). From the numerical value $u = 0{\cdot}243$ (this work) it is immediately clear that the idealization of isolated octahedra is not a very realistic one; the chlorine ions are only slightly closer to Sn (0·243 Å) than to the octahedral holes (0·257 Å) at ($\frac{1}{2}$00).

The structure described here is closely related to the perovskite (*e.g.* $SrTiO_3$) and the elpasolite (*e.g.* K_2NaAlF_6) structures. In the first case all the octahedral positions at (000) and ($\frac{1}{2}$00) are occupied by the same ions (*e.g.* Ti), and $u = \frac{1}{4}$ by symmetry. It is of course more appropriate to describe this structure as a P lattice with $a = \frac{1}{2}a_0$ (Fig. 1, Table 1). In the elpasolites the two octahedral positions are occupied by different ions (*e.g.* Na, Al).

All the structures mentioned above are unstable with respect to displacive phase transitions which have been investigated mostly for the perovskites. In the high-temperature phase of K_2SnCl_6, a librational model of the MX_6 octahedra was deduced from X-ray photographs and neutron experiments (Boysen, Ihringer, Prandl & Yelon, 1976). It is suggested that the librational motion of the MX_6 octahedra plays an important role in the phase transitions of such compounds: Morfee, Staveley, Walters & Wigley (1960) and other authors (Sasane, Nakamura & Kubo, 1970; Jeffrey, 1972; Boysen, Ihringer, Prandl & Yelon, 1976: Winter, Rössler, Bolz & Pelzl, 1976; Boysen,

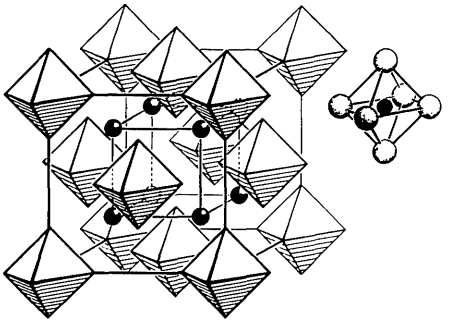

Fig. 1. K_2PtCl_6 structure (from D'Ans-Lax, 1970): small spheres, K; octahedra, $PtCl_6$.

Table 1. *Positional and thermal parameters for* K_2SnCl_6 *at* 300 K

Lattice constant $a = 9{\cdot}988$ Å

8 K in (*c*)	(0·25, 0·25, 0·25) $u_{11} = 0{\cdot}054$ (1)	
4 Sn in (*a*)	(0, 0, 0) $u_{11} = 0{\cdot}0206$ (3)	
24 Cl in (*e*)	[0·2407 (2), 0, 0] $u_{11} = 0{\cdot}021$ (1)	$u_{22} = 0{\cdot}082$ (2)

The thermal parameters in Å^2 are the mean-square displacements in the directions of the corresponding axes. To get the B_{lk} parameter, multiply by $8\pi^2$.

0567-7394/80/010089-08$01.00

1977; Ihringer, 1977) explain the transition in K_2SnCl_6 at $T_{c1} = 261$ K by the softening of a rotary lattice mode. A direct observation of this mode in the cubic phase of K_2SnCl_6 by inelastic neutron scattering is reported by Boysen (1977) and Vogt (1979). The lattice dynamics of R_2MX_6 compounds were studied for the following systems: K_2ReCl_6 by O'Leary & Wheeler (1970), also more recently by Lynn, Patterson, Shirane & Wheeler (1978); Cs_2UBr_6 by Chodos & Satten (1975); and Cs_2SiF_6 by Patterson & Lynn (1979).

In perovskites many of the displacive phase transitions from the cubic to the tetragonal or orthorhombic phase are associated with rotations of the MX_6 octahedra. Dénoyer, Comès, Lambert & Guinier (1974) and Dénoyer (1977) observed a streak system caused by a rotational mode on X-ray photographs of $NaNbO_3$.

We will see that the relationship between the R_2MX_6 and the perovskite structures yields closely related atomic displacement fields for the energetically lowest rotational modes of the octahedra. However, besides this common feature, each structure shows a second characteristic diffuse system in X-ray photographs. In the perovskites RMX_3 there are diffuse planes caused by the one-dimensional M chains. In K_2SnCl_6 we find diffuse scattering along the Σ direction (Γ–K–X; *c.f.* Fig. 4, Fig. 5) which can be explained by a low-lying transversal acoustical mode.

2. High-temperature structure

2.1. *Experimental*

Diffraction data were measured with filtered Mo $K\alpha$ radiation on a Siemens three-circle diffractometer operated in the $\theta/2\theta$ scan mode ($\sin\theta/\lambda \leq 1{\cdot}2$ Å^{-1}). Two data sets (referred to as DS1 and DS2 in the following) of 1200 reflections each were taken from two different octahedral crystals both with 0·5 mm diameter. For the numerical absorption correction, the distances between the boundary crystal faces were measured optically.

2.2. *Data reduction and structure refinements*

The absorption correction, data reduction and structure refinement was performed with the program *SHELX* 76 (Sheldrick, 1975). Equivalent reflections in both data sets were merged to give 264 and 266 independent reflections.

Scattering curves for the Cl^-, K^+ and Sn^{4+} ions were taken from *International Tables for X-ray Crystallography* (1974). Refinements with the final residuals $R = 0{\cdot}047$, $R_w = 0{\cdot}035$ for DS1 and $R = 0{\cdot}039$, $R_w = 0{\cdot}033$ for DS2 were computed with the full data sets and weights from counting statistics. The final parameters of DS1 and DS2 agree within their standard deviations (e.s.d.), the Cl x/a and the Sn thermal parameter within 2 × e.s.d. The parameters from the second data set are listed in Table 1.

The results agree well with those derived by Lerbscher & Trotter (1976) from X-ray and Boysen & Hewat (1978) from neutron powder data. The bond-length correction (Cruickshank, 1956) for the librating Cl ions gives 5·8° as the amplitude of the rotation angle, the corrected Cl parameter is 0·2434 (4).

In DS2 there are four reflections with $F_o - F_c$ greater than 2σ: 111, 002, 004, 044. The 111 and 002 reflections are assumed to be of poor quality because they are inconsistent with those of DS1, the strongest reflections, 004 and 044, in both DS1 and DS2 are weakened by extinction. Omitting these four reflections improved the residuals to $R = 0{\cdot}028$, $R_w = 0{\cdot}025$, and refinement shifted the parameters of Table 1 by less than 2 × e.s.d. in the direction of the results obtained with the first data set. The Sn thermal parameter was shifted about 6 × e.s.d. The final R was 0·022, the refined weighting scheme of $3{\cdot}5/\sigma^2$ gave $R_w = 0{\cdot}019$.

2.3. *Difference electron densities*

The difference-Fourier chart of the plane (0yz) in Fig. 2 was computed with the second data set (DS2) with the four reflections 111, 002, 004, 044 omitted.* Fourier charts usually suffer from series termination errors. In order to test their influence on the difference charge shown in Fig. 2, the computation was repeated using reflections only up to $\sin\theta/\lambda = 0{\cdot}90$. The resulting map shows the same details as Fig. 2 computed from the complete data set, the only difference being that the extrema are less pronounced. They represent, therefore, true information on the charge distribution. The density modifications along the principal axes of the Cl and Sn ions indicate that the anisotropic temperature factors in the harmonic approximation are not sufficient to describe the displacements. The density maxima near the Cl and Sn ions parallel to the bond Sn—Cl give evidence for an acoustic phonon of low energy. Note that the maxima of the Cl ions perpendicular to the bond have no analog near the Sn ions. Therefore, the arc-shaped maxima around the Sn ions may be produced by the librating octahedra. Another reason for these maxima could be modification of the electronic density by covalent bonds between the ions of the octahedra. In the light of

* Lists of the structure factors for the three refinements, the list of resulting parameters and the difference-Fourier chart computed with the full data set DS2 have been deposited with the British Library Lending Division as Supplementary Publication No. SUP 34667 (9 pp.). Copies may be obtained through The Executive Secretary, International Union of Cystallography, 5 Abbey Square, Chester CH1 2HU, England.

inelastic neutron measurements (Boysen, 1977; Vogt, 1979) which verify the soft librational mode along the direction Δ (see Fig. 5), I favor the first explanation.

3. Diffuse background in X-ray single-crystal photographs

X-ray single-crystal photographs of K_2SnCl_6 exhibit two systems of strong, diffuse scattering. In Fig. 3 the first system shows small streaks parallel to the principal axes along the direction $\Delta(\Gamma \rightarrow X)$ (see Fig. 4, Fig. 5). The streaks of highest intensity connect odd-indexed reflections. There are no streaks in the direction [001] between reflections indexed *hhl*. The intensity variation

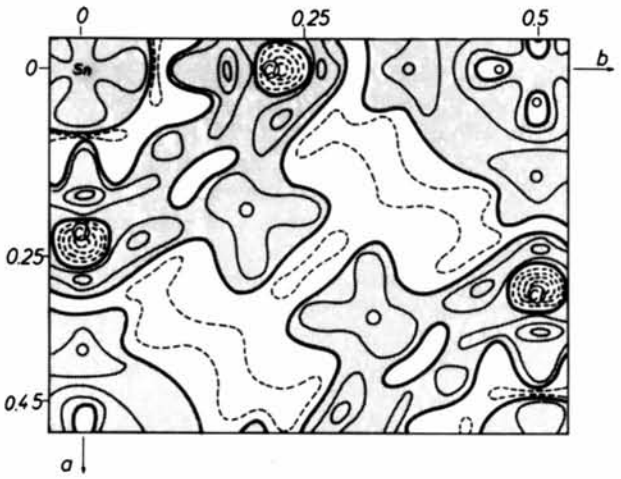

Fig. 2. Difference-Fourier density map in the (001) plane of K_2SnCl_6. The dotted regions are positive areas, broken lines denote negative contours. The density contour lines are separated by 30 units, where 160 units = 1 e/Å^3.

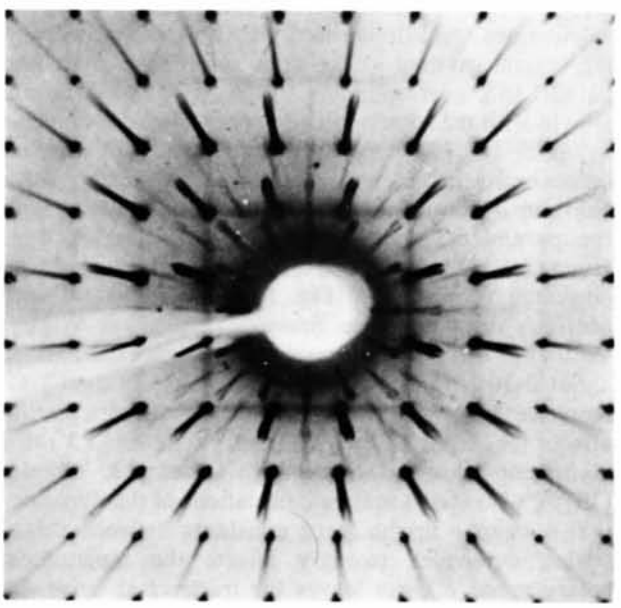

Fig. 3. Precession photograph from K_2SnCl_6 at room temperature. First layer of the [001] zone with filtered Mo $K\alpha$ radiation. The a^* axis lies horizontal.

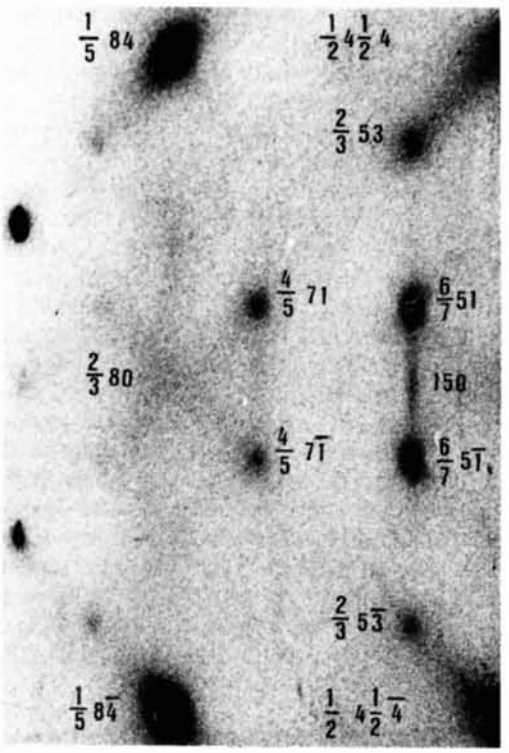

(*a*)

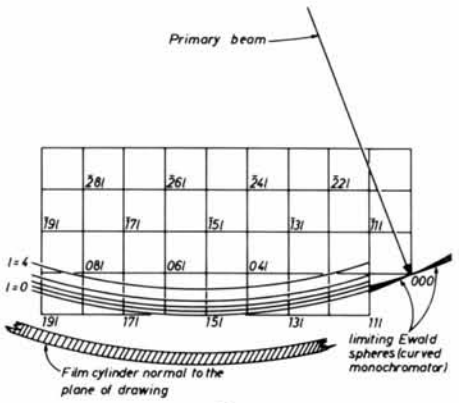

(*b*)

Fig. 4.(*a*) Diffuse X-ray scattering pattern of a fixed K_2SnCl_6 crystal with [001] parallel to the incident beam (Mo $K\alpha_1$ radiation; curved quartz monochromator). The vertical diffuse lines correspond to the scattering from the (010) planes along the direction Δ. The broader inclined diffuse lines are acoustic scattering starting from the neighboring Bragg points 044 and 080 along the direction Σ. (*b*) Geometric features of (*a*). The reciprocal space and the intersections of the mean Ewald sphere with the layers ($l = 0, \ldots, 4$) are projected onto the (001) plane. The primary beam lies within the (001) plane normal to the film cylinder.

along the streaks is small. In real space we therefore expect correlations in planes only. The small diameter of the streaks indicates a long extension of the correlations within the planes.

The second system, pointing along the Σ direction (Γ–K–X) (Fig. 4), is broader than the first one. Its intensity is proportional to the intensity of the corresponding Bragg reflections and therefore it must be due to acoustic phonons with neighboring atoms moving in phase. Fig. 5 shows the diffuse scattering with respect to the Brillouin zones.

To interpret both systems by low-lying phonons, the basis vectors of the normal-mode displacement fields were evaluated for the direction Δ (Figs. 5, 6*a*) and Σ (Fig. 6*b*) by the projections operator technique (Maradudin & Vosko, 1968). Table 2(*a*) and (*b*) shows the eigenvector-dependent part of the inelastic scattering factors of the Cl ions for all normal modes. Rigid octahedra are assumed in these calculations. The A_2 mode completely describes the observed extinction rules and the intensity of the streak system in the Δ direction. The second system in the vicinity of even-indexed reflections shows maximal intensity along [110] for $hh\bar{l}$ reflections with $h = 4n$, and zero intensity along the same direction for hhl reflections. The transverse acoustic B_1 mode along Σ explains these diffuse intensities. At the X point, the A_{2g} mode is compatible with the $A_2(\Delta)$ mode as well as with a $B_1(\Sigma)$ mode.

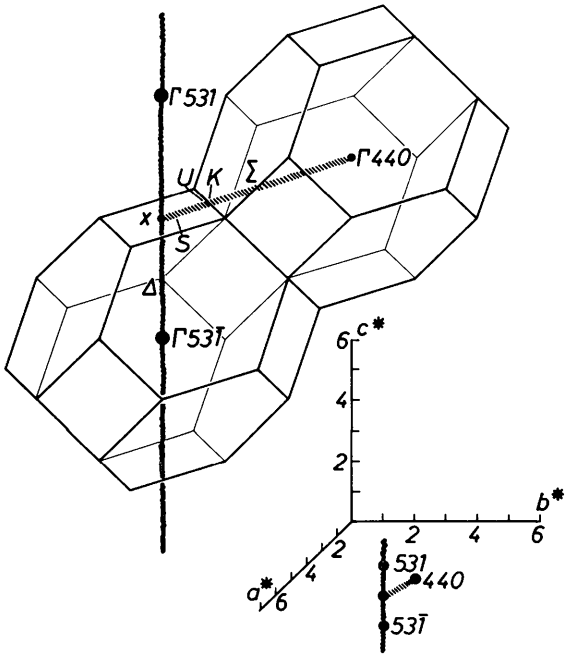

Fig. 5. Σ and Δ directions in neighboring Brillouin zones for the face-centered cubic lattice in the vicinity of even- and odd-indexed reflections.

In Fig. 7 a cross section through the Cl_6 octahedra is shown for three typical situations: for all octahedra in their time-averaged position ($\varphi = 0$); for an in-phase rotation and for an anti-phase rotation of nearest octahedra. The second and third cases correspond to $A_2(\Delta)$ and $E(\Delta)$ modes, respectively. For the $A_2(\Delta)$ mode there is only little steric hindrance up to a rotation of 14° (for the Cl ionic radius chosen), for the $E(\Delta)$ mode, however, repulsion occurs even at a small rotation angle. From this one can conclude that in an $A_2(\Delta)$ mode displacement there are only weak forces between the Cl ions belonging to neighbouring octahedra, therefore the mode should be very soft.

Octahedra of different planes are coupled by the K ions between them. The shortest K–Cl distance is 3·54 Å but the sum of the ionic radii is only 3·14 Å. Therefore, the octahedra can rotate around [001] by about 14° before K and Cl come into direct contact. This may explain the weak coupling of adjacent planes for the A_2-mode displacement field.

To get more quantitative information the lattice-energy calculations of Morfee, Staveley, Walters & Wigley (1960) were redone and generalized beyond a strictly electrostatic approach by adding a Born–Meyer potential term

$$\Phi_{ab} = -q_a q_b / r_{ab} + \lambda_{ab} \exp(-r_{ab}/\rho_{ab}).$$

Φ_{ab} denotes the potential energy of two particles a and b with charges q_a, q_b at a distance r_{ab}. λ_{ab} and ρ_{ab} are the repulsive parameters. The lattice sums of the Coulombic part of the energy were evaluated by Ewalds method (Ewald, 1921; Leibfried, 1955), the repulsive parts were summed in real space. Two sets of calculations were done: the first with the octahedra in the crystal rotating in the same sense around an axis parallel to b corresponding to the $A_{2g}(\Gamma)$ mode and a second with the rotation in adjacent planes out of phase by 180° [$A_{2g}(X)$ mode]. The parameter of greatest influence on the potential turned out to be the repulsive constant ρ_{ab} between the K and Cl ions. Starting with the parameter reported for KCl crystals (Born & Huang, 1954), $\rho_{KCl} = 0{\cdot}324$, the potential shows a deep minimum at $\gamma = 20°$ [Fig. 8(1)] which agrees with Morfee's result (Morfee, Staveley, Walters & Wigley, 1960), but this minimum vanishes if ρ_{KCl} is raised above about 0·36 [Fig. 8(2)]. A similar change in the Cl–Cl repulsive parameter of neighboring octahedra hardly affects the depth of the minimum for the $A_{2g}(X)$ displacement field. This agrees with O'Leary & Wheeler (1970), who stated in their calculations of the dynamics that a change in the force constants between neighboring octahedra strongly affects the longitudinal rotary mode E_g, but leaves the transversal mode A_{2g} unaffected.

There is no significant difference in energy between an in-phase rotation of all octahedra [$A_{2g}(\Gamma)$] and an

alternating rotation in adjacent planes [$A_{2g}(X)$]. This indicates that neighboring planes are nearly uncoupled for this type of motion. We therefore expect a flat dispersion curve for the $A_2(\Delta)$ mode, which is in agreement with the X-ray observation described earlier [Fig. 8(3)]. No minimum in the energy appears if adjacent octahedra in a plane are tilted in opposition to one another, according to the E_g mode at the X point.

In this simple model the numerical value of ρ is crucial for deciding which structure is established after cooling the crystal: the tetragonal structure with $P4/mnc$, resulting from the $A_{2g}(X)$ condensation; or an orthorhombic structure with four molecules in the unit cell (Kugler, 1979). Such a structure could be explained by two successive phase transitions: first an $A_{2g}(X)$ condensation with wave vector (001), followed by a second rotation of the octahedra with wave vector (010) around an axis [010] normal to that of the first rotation. The symmetry $P4/mnc$ after the first transition would be reduced by the second to $Pnnn$.

However, this model cannot explain details of the transitions, *e.g.* that at $T_{c1} = 261$ K we find an $A_{2g}(X)$ and not an $A_{2g}(\Gamma)$ condensation; this could be, for example, because all ions are treated as point charges and their polarizability remains unconsidered.

4. Discussion

We have found that in K_2SnCl_6 crystals the 'in-phase' rotation of neighboring octahedra in (001) ↻ planes minimizes the lattice energy. From the narrow streaks, on the other hand, long-range correlations of the rotation in these planes is deduced, whereas the coupling between adjacent planes is weak. There is indeed a small smooth increase of the streak intensity around the X point which indicates a slight decrease of the mode energy $\omega(q)$ at X (Ihringer, 1977), that is, the antiphase rotation of adjacent planes is preferred.

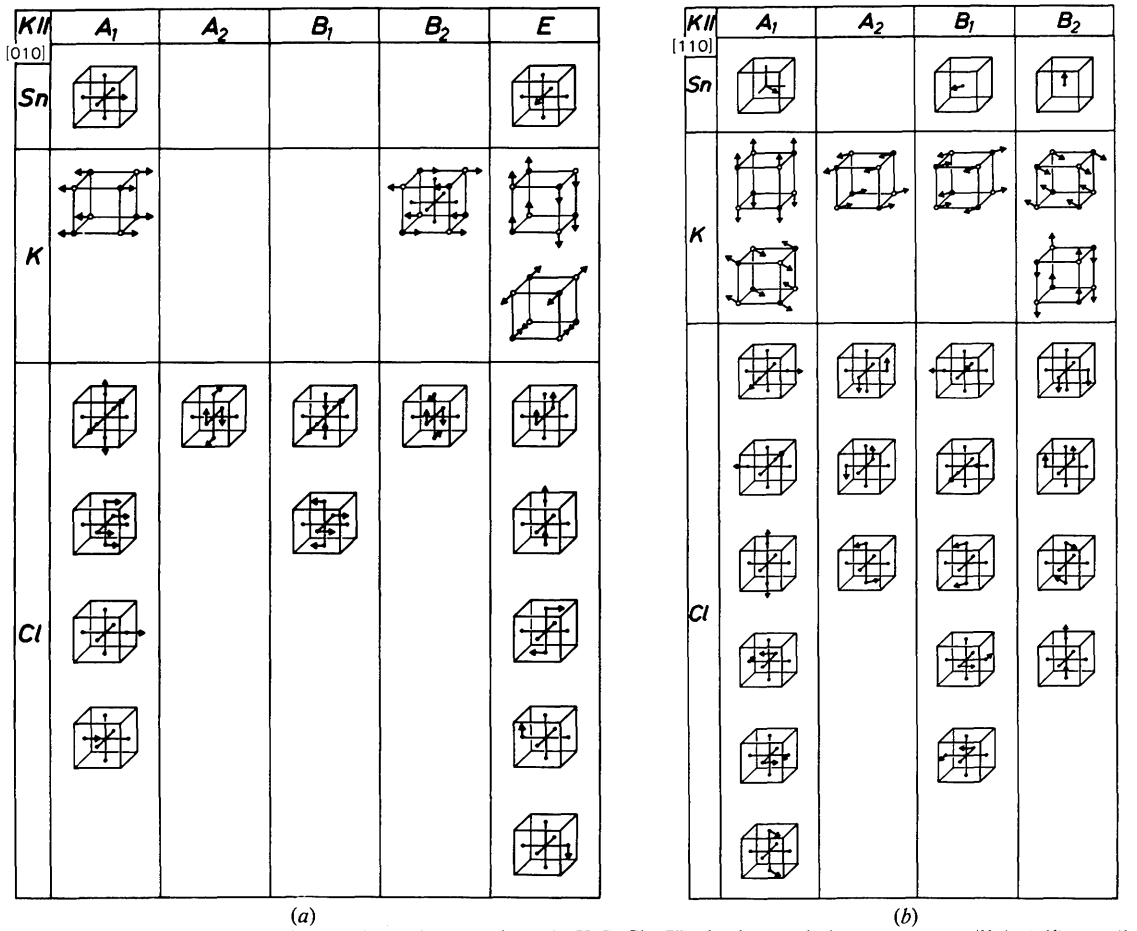

Fig. 6. Normal-mode displacement fields for the lattice complexes in K_2SnCl_6. The basic translation vectors are $(\frac{1}{2}\frac{1}{2}0)$, $(0\frac{1}{2}\frac{1}{2})$ and $(\frac{1}{2}0\frac{1}{2})$, so ○ and ● denote translation-equivalent K ions. A translation along **r** yields a phase shift of $\cos 2\pi\mathbf{k}.\mathbf{r}$; **k** is the wave vector. (*a*) **k** lies in the direction Δ parallel to the *b* axis, its point group is $4mm$. The K^+ displacements with a phase factor -1 between equivalent K^+ ions are shown for **k** near the X point. For the two-dimensional representation E of each displacement field, only one basis vector is shown, the second can be derived by exchanging the *a* and *c* axes. (*b*) **k** lies in the Σ direction (Γ–K–X; Fig. 5). The K^+ displacements are shown for $\mathbf{k} = (\frac{1}{2}\frac{1}{2}0)$.

Table 2. *Mode inelastic structure factor $\hat{F}$ for the rigid $SnCl_6$ octahedra of K_2SnCl_6 as a function of the wave vector* **q** *for different normal modes*

$\hat{F} = \sum [\mathbf{k}.\mathbf{e}_j(\lambda\mathbf{q})]\, e^{i\mathbf{k}\mathbf{r}_j}$, where $\mathbf{e}_j(\lambda\mathbf{q})$ is the eigenvector of the jth atom for phonon branch λ of the wavevector **q**, $\mathbf{k} = \mathbf{H} + \mathbf{q}$, **H** is the Bragg point vector and $\mathbf{r}_j$ is the position of the jth atom.

(*a*) Wave vectors parallel to [010] along the direction Δ of the Brillouin zone, δ is the deviation of the anion parameter from 1/4

$\Delta\,\mathbf{k} \parallel [010]$			Acoustical modes		Optical modes	
h	k	l	$A_1(\Delta)$ $(k+q)\times$	$E^{(2)}(\Delta)$ $h\times$	$A_2(\Delta)$	$E^{(1)}(\Delta)$
$4n$	$4n$	$4n$	$2+\cos(\pi/2)\,q$		0	$-l\cos(\pi/2)\,q$
$4n+2$	$4n$	$4n$	$\cos(\pi/2)\,q$		$2\pi hl\delta$	$-l\cos(\pi/2)\,q$
$4n+2$	$4n$	$4n+2$	$-2+\cos(\pi/2)\,q$		0	$-l\cos(\pi/2)\,q$
$4n$	$4n+2$	$4n$	$-2+\cos(\pi/2)\,q$		0	$l\cos(\pi/2)\,q$
$4n+2$	$4n+2$	$4n$	$-\cos(\pi/2)\,q$		$2\pi hl\delta$	$l\cos(\pi/2)\,q$
$4n+2$	$4n+2$	$4n+2$	$-2-\cos(\pi/2)\,q$		0	$l\cos(\pi/2)\,q$
$4n+1$	$4n+1$	$4n+1$	$-\sin(\pi/2)\,q$		$l-h$	$-k-q+l\sin(\pi/2)\,q$
$4n-1$	$4n+1$	$4n+1$	$-\sin(\pi/2)\,q$		$l+h$	$-k-q+l\sin(\pi/2)\,q$
$4n-1$	$4n+1$	$4n-1$	$-\sin(\pi/2)\,q$		$l-h$	$-k-q+l\sin(\pi/2)\,q$
$4n+1$	$4n-1$	$4n+1$	$\sin(\pi/2)\,q$		$l-h$	$-k-q-l\sin(\pi/2)\,q$
$4n-1$	$4n-1$	$4n+1$	$\sin(\pi/2)\,q$		$l+h$	$-k-q-l\sin(\pi/2)\,q$
$4n-1$	$4n-1$	$4n-1$	$\sin(\pi/2)\,q$		$l-h$	$-k-q-l\sin(\pi/2)\,q$

(*b*) Wavevectors **q** parallel to [110] along the direction Σ of the Brillouin zone.

$\Sigma\mathbf{k} \parallel [110]$			Acoustical modes			Optical modes	
h	k	l	$A_1(\Sigma)$ $(h+k+2q)\times$	$B_1(\Sigma)$ $(h-k)\times$	$B_2(\Sigma)$ $l\times$	$A_2(\Sigma)$	$E(\Sigma)$
$4n$	$4n$	$4n$	$1+2\cos(\pi/2)\,q$			0	$(h-k)\sin(\pi/2)\,q$
$4n+2$	$4n$	$4n$	1			$l\sin(\pi/2)\,q$	$(h+k)\sin(\pi/2)\,q$
$4n+2$	$4n+2$	$4n$	$1-2\cos(\pi/2)\,q$			0	$(h-k)\sin(\pi/2)\,q$
$4n$	$4n$	$4n+2$	$-[1-2\cos(\pi/2)\,q]$			0	$(h-k)\sin(\pi/2)\,q$
$4n+2$	$4n$	$4n+2$	1			$-l\sin(\pi/2)\,q$	$(h+k)\sin(\pi/2)\,q$
$4n+2$	$4n+2$	$4n+2$	$-[1+2\cos(\pi/2)\,q]$			0	$(h-k)\sin(\pi/2)\,q$
$4n+1$	$4n+1$	$4n+1$	$-2\sin(\pi/2)\,q$			$h-k$	$(h-k)\cos(\pi/2)\,q$
$4n-1$	$4n+1$	$4n+1$	0			$h-k+l\cos(\pi/2)\,q$	$(h+k)\cos(\pi/2)\,q$
$4n-1$	$4n-1$	$4n+1$	$2\sin(\pi/2)\,q$			$h-k$	$(h-k)\cos(\pi/2)\,q$
$4n+1$	$4n+1$	$4n-1$	$-2\sin(\pi/2)\,q$			$-(h-k)$	$(h-k)\cos(\pi/2)\,q$
$4n-1$	$4n+1$	$4n-1$	0			$-(h-k+l)\cos(\pi/2)\,q$	$(h+k)\cos(\pi/2)\,q$
$4n-1$	$4n-1$	$4n-1$	$2\sin(\pi/2)\,q$			$-(h-k)$	$(h-k)\cos(\pi/2)\,q$

In the perovskites on the other hand there are planes perpendicular to [100] with rigid octahedra in anti-phase rotation that are linked by a common anion. It is a particular feature of the rotational modes that they induce nearly identical anion-displacement fields in both structures. The in-phase rotation of neighboring $SnCl_6$ groups in K_2SnCl_6 implies for the octahedral gaps between them an anti-phase rotation, which leaves this 'empty' octahedron nearly undistorted (Fig. 9*a*). These rotational modes do not affect the cations, therefore it is insignificant whether the octahedron is 'empty' or 'filled'. For the analogy with the perovskites it is important that all octahedra remain essentially undistorted, that is, we find in both structures an identical scheme of corner-linked tilted X_6 octahedra. In consequence, the distribution of the diffuse X-ray intensity due to this type of motion is nearly identical in both cases. The streaks in cubic perovskites extend parallel to the principal axis from the R to the M point of the Brillouin zone of the primitive cubic lattice. The coordinates of the R and M points are $(h+\frac{1}{2}, k+\frac{1}{2}, l+\frac{1}{2})$ and $(h+\frac{1}{2}, k+\frac{1}{2}, l)$. Referred to the reciprocal lattice of K_2SnCl_6 with a^* (perovskite) $= 2a^*$ (K_2SnCl_6), these points are indexed $(2h+1, 2k+1, 2l+1)$ and $(2h+1, 2k+1, l)$, respectively. So the R point in the perovskite cell corresponds to an odd-indexed

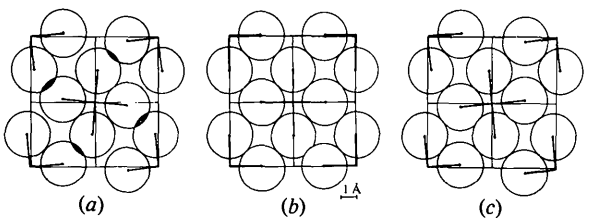

Fig. 7. Displacement of the Cl ions in the (001) plane. The ionic radii ($r_{Cl} = 1{\cdot}81$ Å) are scaled with the unit cell ($a = 10$ Å). (*a*) Anti-phase rotation of adjacent octahedra. (*b*) Octahedra at rest with $\varphi = 0$. (*c*) In-plane rotation of adjacent octahedra; neighboring octahedra may rotate with little hindrance up to $\varphi \simeq 15°$.

reciprocal-lattice point in the f.c.c. R_2MX_6 cell and the M point to the X point of the latter. The streaks of the perovskite structure from R to M correspond to those along Δ from Γ to X between the odd-indexed reflections of the R_2MX_6 cell.

The streaks along Δ between the even-indexed reflections of the R_2MX_6 structure have no analog in the perovskites, so they display one difference between the structures. The inelastic structure factor for those streaks is proportional to the deviation of the u parameter from 1/4 (see Tables 1 and 2). This means that the streaks are caused by the difference between the diameters of the M-filled MX_6 and the empty X_6 octahedra in the R_2MX_6 structure.

As a further difference we expect that the rotational mode in perovskites is of higher energy than in R_2MX_6, because higher librational amplitudes expand the linked perovskite octahedra, that is, the rotation of the octahedra couples with an internal mode of the octahedra. The 'filled' MX_6 octahedra in R_2MX_6 rotate as rigid units until considerable steric hinderance sets in ($\varphi \simeq 15°$). The empty octahedra may expand, since the Coulomb force is repelling the Cl ions and since no covalent forces are holding them together.

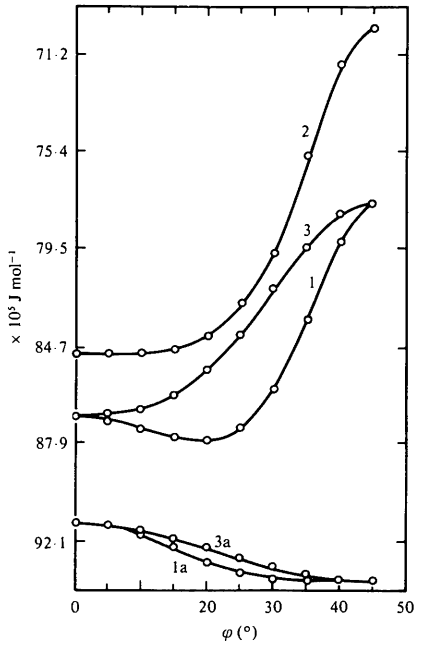

Fig. 8. Electrostatic and hard-core lattice energy as a function of the rotation angle of the octahedra for an in-phase rotation of adjacent octahedra in a plane. Parameters are the Born–Meyer repulsive constants ρ_{12}, λ_{12} for the K–Cl and Cl–Cl potentials. $\Phi_{12} = -q_1 q_2/r_{12} + \lambda_{12} \exp(-r_{12}/\rho_{12})$, q_1 and q_2 are the charges with distance vector r_{12}. Curve (1): $\lambda_{KCl} = 3{\cdot}63$, $\rho_{KCl} = 0{\cdot}324$ (taken from the KCl structure); the Cl–Cl repulsive parameters are arbitrary, $\lambda_{ClCl} = 4{\cdot}0$, $\rho_{ClCl} = 0{\cdot}363$. Curve (2) shows that the minimum vanishes if the ρ_{KCl} parameter is raised to 0·37. The contribution of the Coulomb energy is shown in Fig. 1(*a*). Curves (3*a*) and (3) show the Coulomb and lattice energy, respectively, for the anti-phase rotation of adjacent octahedra in a plane. The repulsive parameters are those of curve (1).

The second diffuse system in the Σ direction in K_2SnCl_6 X-ray photographs is assumed to be typical for R_2MX_6 structures. The $B_1(\Sigma)$ mode elongates adjacent MX_6 octahedra normal to their distance vector and the 'empty' corner-linked X_6 octahedra are distorted (Fig. 9*b*), so one would expect that in structures with all the octahedra filled this type of motion needs a higher excitation energy. On the other hand, we cannot expect to find in R_2MX_6 photographs the diffuse planes characteristic of the perovskite structure, because the correlated M-chain movement requires corner-linked MX_6 octahedra.

To get a model for the phase transition in K_2SnCl_6 at $T_{c1} = 261$ K we assume that the potential with respect to the octahedra rotation exhibits two minima located symmetrically to the average position at $\varphi = 0$. The double-minimum potential is anharmonic; the difference-Fourier map confirms that the thermal ellipsoids of the harmonic approximation are insufficient to describe the librational amplitudes of the octahedra. At $T > T_{c1}$, the energy of the torsional mode is well above the potential barrier at $\varphi = 0$.

The broad potential well yields large amplitudes and the repulsion of the Cl ions by the K ions stabilizes the lattice. With decreasing temperature the lattice constant decreases. This implies an increase in the Cl parameter, u, when rigid octahedra are assumed. The lattice-energy calculations show that with increasing u and decreasing lattice constant a the potential well at $\varphi = 0$ is raised, so we expect the first phase transition at T_{c1} when the mode energy is insufficient to penetrate the potential barrier.

I wish to thank Professor H. Jagodzinski and Professor W. Prandl for many helpful discussions, and Dipl.-Phys. W. Kugler and Dipl.-Phys. K. Vogt for communicating results prior to publication.

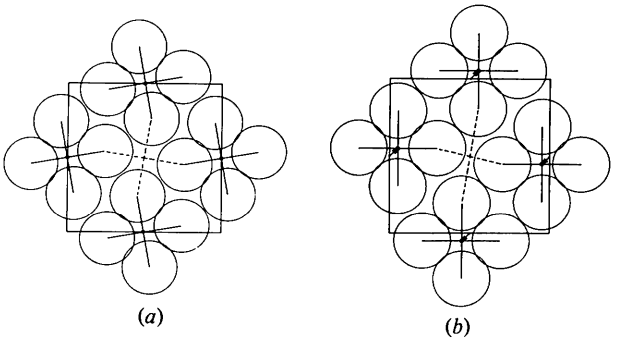

Fig. 9. Deformation of the 'empty' octahedra in K_2SnCl_6 between the rotated $SnCl_6$ octahedra (*a*) for the $A_2(\Delta)$ mode [$\mathbf{k} = (010)$] and (*b*) for the $B_1(\Sigma)$ mode [$\mathbf{k} = (\frac{1}{2}\frac{1}{2}0)$].

References

BORN, M. & HUANG, K. (1954). *Dynamical Theory of Crystal Lattices*. Oxford: Clarendon Press.

BOYSEN, H. (1977). *Untersuchungen an den strukturellen Phasenübergängen des K_2SnCl_6 mit Hilfe von Neutronenbeugungsmethoden*. Dissertation, Univ. München.

BOYSEN, H. & HEWAT, A. W. (1978). *Acta Cryst.* B**34**, 1412–1418.

BOYSEN, H., IHRINGER, J., PRANDL, W. & YELON, W. (1976). *Solid State Commun.* **30**, 1019–1024.

CHODOS, S. L. & SATTEN, R. A. (1975). *J. Chem. Phys.* **62**, 2411.

CRUICKSHANK, D. W. J. (1956). *Acta Cryst.* **9**, 757.

D'ANS-LAX (1970). *Taschenbuch für Chemiker und Physiker*, Vol. III. Berlin: Springer-Verlag.

DÉNOYER, F. (1977). *Etude des Transitions de Phase Structurale de $NaNbO_3$ par les Rayons X et Diffusion Inélastique des Neutrons*. Thesis, Univ. Paris-Sud, Centre d'Orsay, France.

DÉNOYER, F., COMÈS, R., LAMBERT, M. & GUINIER, A. (1974). *Acta Cryst.* A**30**, 423–430.

EWALD, P. P. (1921). *Ann. Phys.* **64**, 250.

IHRINGER, J. (1977). *Röntgenographische Untersuchungen der Hochtemperaturstruktur und der Phasenumwandlungen von K_2SnCl_6*. Dissertation, Univ. München.

International Tables for X-ray Crystallography (1974). Vol. IV. Birmingham: Kynoch Press.

JEFFREY, K. R. (1972). *J. Magn. Reson.* **7**, 184–195.

KUGLER, W. (1979). Private communication and to be published.

LEIBFRIED, G. (1955). *Encyclopedia of Physics*, Vol. 7, part 1, edited by S. FLÜGGE, p. 132. Berlin: Springer-Verlag.

LERBSCHER, J. A. & TROTTER, J. (1976). *Acta Cryst.* B**32**, 2671–2672.

LYNN, J. W., PATTERSON, H. H., SHIRANE, G. & WHEELER, R. G. (1978). *Solid State Commun.* **27**, 859.

MARADUDIN, A. A. & VOSKO, S. H. (1968). *Rev. Mod. Phys.* **40**, 1.

MORFEE, R. G. S., STAVELEY, L. A. K., WALTERS, S. T. & WIGLEY, D. L. (1960). *J. Phys. Chem. Solids*, **13**, 132–144.

O'LEARY, G. P. & WHEELER, R. G. (1970). *Phys. Rev. B*, **1**, 4409.

PATTERSON, H. H. & LYNN, J. W. (1979). Submitted for publication.

SASANE, A., NAKAMURA, D. & KUBO, M. (1970). *J. Magn. Reson.* **3**, 76–83.

SHELDRICK, G. M. (1975). *SHELX – version of June 75*. University Chemical Laboratory, Lensfield Road, Cambridge, England.

VOGT, K. (1979). Private communication and to be published.

WINTER, J., RÖSSLER, K., BOLZ, J. & PELZL, J. (1976). *Phys. Status Solidi*, **74**, 193–198.

Acta Cryst. (1980). A**36**, 96–103

An Electron Diffraction Study of the Molecular Structure of the Sodium Chloride Dimer

BY H. MIKI, K. KAKUMOTO,* T. INO, S. KODERA AND J. KAKINOKI†

Department of Physics, Faculty of Science, Osaka City University, Sugimoto-cho, Sumiyoshi-ku, Osaka 558, *Japan*

(*Received* 29 *May* 1978; *accepted* 7 *August* 1979)

Abstract

The structure of sodium chloride has been studied by gas-phase electron diffraction using photographic plates designed for high-temperature work [Kakumoto, Ino, Kodera & Kakinoki (1977). *J. Appl. Cryst.* **10**, 100–103]. The molecular structure at about 1130 K has been determined by an analysis based on the new complex scattering factors for Na^+ and Cl^- calculated recently by the present authors. The radial distribution function shows the existence of a considerable amount of dimer molecules in the vapor. The structures of the monomer and dimer have been analyzed by a least-squares method assuming that the dimer is of a planar diamond shape: for monomer r_a(Na–Cl) = 2·392 ± 0·028, for dimer r_a(Na–Cl) = 2·515 ± 0·017, r_a(Cl–Cl) = 3·893 ± 0·021 Å, ∠ClNaCl = 101·4 ± 0·8°. The present study indicates that the Na–Cl distance of the dimer is longer than that of the monomer and the determined structure parameters differ appreciably from existing theoretical predictions.

Introduction

The structure of alkali halide molecules at high temperatures was studied by electron diffraction for the first time by Maxwell, Hendricks & Mosley (1937). They determined the internuclear distances in various

* Present address: Koyo Research Center, Kokubu, Kashiwara-shi, Osaka 582, Japan.

† Present address: Setsunan University, Ikeda-naka, Neyagawa-shi, Osaka 572, Japan.

0567-7394/80/010096-08$01.00